Effective-density-matrix approach for intersubband plasmons coupled to a cavity field: Electrical extraction and injection of intersubband polaritons

M. Lagrée,[1,*] M. Jeannin,[2] G. Quinchard,[1] S. Pes,[1] A. Evirgen,[1] A. Delga,[1] V. Trinité,[1,†] and R. Colombelli[2,‡]

[1] *III-V Lab, Campus Polytechnique, 1, Avenue Augustin Fresnel, RD 128, Palaiseau cedex 91767, France*
[2] *Centre de Nanosciences et de Nanotechnologies (C2N), CNRS UMR 9001, Université Paris-Saclay, Palaiseau 91120, France*

The main technological obstacle hampering the dissemination of modern optoelectronic devices operating with large light-matter coupling strength Ω is an in-depth comprehension of the carrier current extraction and injection from and into strongly coupled light-matter states, the so-called polaritonic states. The main challenge lies in modeling the interaction between excitations of a different nature, namely bosonic excitations [the plasmonic intersubband (ISB) excitations] with fermionic excitations (the electrons within the extraction or injection subband). In this work, we introduce a comprehensive quantum framework that encompasses both the ISB plasmonic mode and the extractor and injector mode, with a specific emphasis on accurately describing the coherent nature of transport. This reveals inherent selection rules dictating the interaction between the ISB plasmon and the extraction and injection subband. To incorporate the dynamics of the system, this framework is combined to a density-matrix model and a quantum master equation, which have the key property to distinguish intra- and intersubband mechanisms. These theoretical developments are confronted to experimental photocurrent measurements from midinfrared quantum cascade detectors ($\lambda = 10 \, \mu$m) embedded in metal-semiconductor-metal microcavities, operating at the onset of the strong light-matter coupling regime ($2\Omega = 9.3$ meV). We are able to reproduce the different features of the photocurrent spectra, notably the relative amplitude evolution of the polaritonic peaks with respect to the voltage bias applied to the structure. These results on extraction allow us to elucidate the possibility to effectively inject electronic excitations into ISB plasmonic states, and thus polaritonic states.

I. INTRODUCTION

The use of electromagnetic resonators like antennas or cavities is an established tool to tailor and improve the properties of optoelectronic devices, whether by increasing the sensitivity, reducing the electronic noise, or improving the wall-plug efficiency. In general, the strategy is to engineer, and typically increase, the interaction strength between light and an electronic transition in matter. However, the interaction strength in practical devices is always limited to a small fraction of the photon or electronic transition lifetimes, which places the device in the so-called *weak-coupling* regime. In contrast, when the light-matter interaction strength overcomes the losses in the system, the latter enters the *strong-coupling* regime. The new constituents of this system are mixed light-matter states

called *polaritons*, which can be formed by hybridizing any polarization-carrying matter excitation and a photon field.

Polariton physics thus emerged as a transverse research field studying the fundamental properties of strongly coupled systems. It revealed a plethora of phenomena, the most recognized being the out-of-equilibrium Bose-Einstein condensation of exciton polaritons [1–3]. However, most experiments on polaritons are performed by optical means, whereas practical devices require electrical injection or extraction of charge carriers. Recent experiments sparked interest in electrical transport in systems under strong light-matter coupling conditions, with the report of increased conductivity in organic molecules [4], or the breakdown of topological protection in quantum Hall systems [5,6]. Intense research effort is thus currently devoted to provide an accurate description of transport in systems strongly coupled to a cavity field.

In this context, intersubband (ISB) polaritons, that originate from the coupling between an intersubband

---

*[*]mathurin.lagree@cea.fr
[†]virginie.trinite@3-5lab.fr
[‡]raffaele.colombelli@c2n.upsaclay.fr

transition in doped semiconductor quantum wells (QWs) and a cavity mode, are of particular interest. They were first reported in 2003 [7] with absorption experiments, and that same year electronic detection of the signature of strong coupling was also reported [8]. Since then, a lot of effort has been devoted to demonstrate nonlinear ISB polariton interaction towards ISB polariton lasers [9,10], with the demonstration of polariton-phonon scattering [11] and more recently, polariton-polariton scattering [12] in an ultrafast pump-probe experiment. ISB polaritons also recently found applications in free-space midinfrared optical devices, such as nonlinear frequency converters [13], amplitude modulators [14], and saturable absorbers and optical limiters [15–17]. However, proposals for electrical injection and electroluminescence of ISB polariton devices [18,19], that were quickly followed by experimental work [20,21], faced the problem of inefficient electrical injection in a polaritonic state. That issue proved insurmountable in the following years [21–24]. Several strategies have been investigated to circumvent the problem, such as studying the transport in resonant tunneling diodes operating in the strong-coupling regime [25], or employing the "reverse" process (photodetection) to elucidate transport mechanisms in polaritonic ISB electronic devices, with experiments on quantum well infrared photodetectors (QWIPs) operating in the strong light-matter coupling regime [26]. In this context, we have recently presented a semiempirical model to describe the electronic photoresponse of quantum cascade detectors (QCDs) operating in the strong light-matter coupling regime [27]. Based solely on classical oscillators, it allowed us to shine light on the polariton-to-electron process, and in particular to conjecture that a direct polariton-to-electron tunnel mechanism may play a major role in such devices. This result was obtained at the expense of great simplifications. In particular, because the model is based on classical theory, it cannot include any consideration on the *coherence* of the involved processes.

Nevertheless, coherence is of major relevance when dealing with systems operating in the strong-coupling regime, and even more so for ISB polaritons, that originate from the coupling between a cavity mode and a collective excitation. ISB transitions, that are more rigorously defined as ISB plasmons [28–30], are collective matter excitations originating from the electronic plasma inside a semiconductor quantum well. They are subject to their own Coulomb interaction, that must be carefully included in their description using the plasmonic effect ω_P of the electronic polarizations. This is in stark contrast to, for instance, exciton polaritons [2,31,32] where the Coulomb interaction is already included in the exciton state and does not need additional treatment, provided exciton-exciton interactions are neglected. An indirect consequence is the presence of *dark states*, that do not couple to the electromagnetic field, but do participate in electronic transport. This has major consequences on the behavior of ISB polariton systems under electrical injection.

In this paper, we propose a quantum description of QCDs based on a density-matrix formalism, that we compare to a complete set of experimental data. Crucially, this approach allows us to describe (de)coherence and dissipation in the system. Our goal is to develop a theoretical description that permits to explain the *electronic extraction* process (photodetection), and that—at the same time—provides a more suitable vantage point to elucidate the more complex *electronic injection* process leading to light emission. We note that a very recent work reports experimental results and proposes an alternative transport model for similar QCD structures operating in the strong-coupling regime [33]. It explicitly retains all the Fermionic degrees of freedom, without performing the bosonisation steps. While similar conclusions are drawn in the photodetection case , our work raises fundamental open questions and presents ways forward to the case of electrically pumped polaritonic light emitters.

In the first part, we develop the model and derive the main observable quantities, notably the photocurrent generated by an exciting external photon field.

In the second part, we validate the theoretical results by studying the photoresponse of quantum cascade detectors operating in the strong-coupling regime as a function of the applied bias. We compare the values obtained in our model with an in-house code based on Ref. [34] that models the electronic transport in a more rigorous way, but does not incorporate the cavity effects [35,36].

In the last part, we discuss the implications of the main assumption at the basis of our model, and extend them to the case of electrical injection.

The system under study is sketched in the central part of Fig. 1. It consists of two electronic subbands confined inside a QW, here represented in momentum space. The second subband is tunnel coupled to the fundamental state of an adjacent QW, and the whole system is embedded inside a cavity. The system can operate as a detector, acting as a QCD (top sketch), when it is excited by a photon that generates a photocurrent. This path is represented by blue arrows. It is also possible to inject electrons in the system (red arrows and bottom sketch), when an electric bias is applied, that can eventually lead to photon emission. In this case the device behaves as a polaritonic LED.

II. AN EFFECTIVE DENSITY-MATRIX APPROACH FOR ELECTRONIC TRANSPORT IN CAVITY-COUPLED QCDS

A. Bosonization of the active optical transition

We start by defining the annihilation and creation operators $c_{\lambda\mathbf{k}}$ and $c^{\dagger}_{\lambda\mathbf{k}}$, the fermionic operators related to the creation and annihilation of electrons in subbands
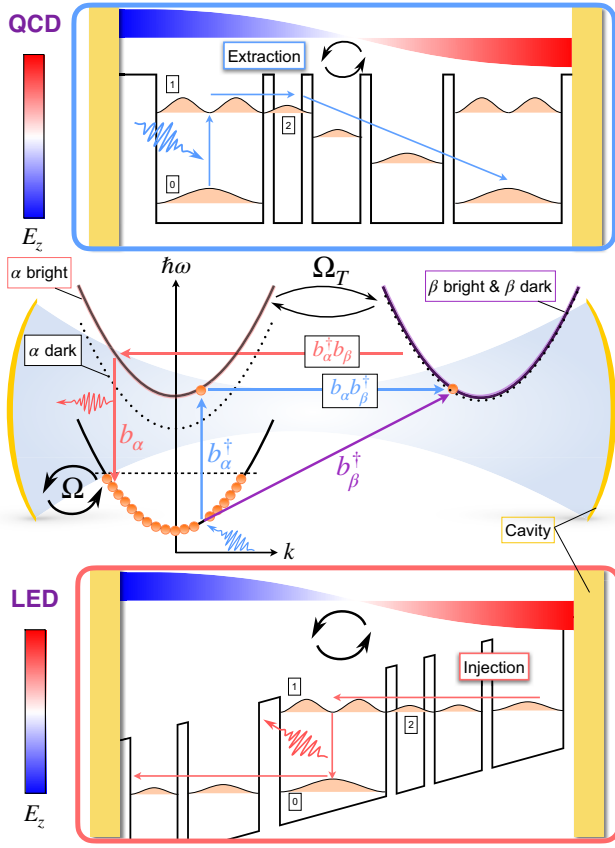
FIG. 1. (Center) Schematic representation of the system in momentum space. Bright and dark states are represented for both α ($0 \to 1$) and β ($0 \to 2$) transitions. Note that the β-bright state is degenerated with the β-dark states. The different relevant operators and their effect on the transport of the excitations are represented. The blue path represents a detection process, whereas the red path represents an injection process. (Top) Typical band structure for a quantum cascade *detector*. The main *extraction* pathway is represented in blue. (Bottom) Typical band structure for a quantum cascade *emitter*. The main *injection* pathway is represented in red. The cavity electric field E_z is also schematically superimposed on the figure.

$\lambda = \{0, 1, 2\}$ (see Fig. 1). We impose $T = 0$ K and we assume that all N electrons are contained inside the 0 subband without external excitation. The one-particle quantum state $|1, \mathbf{k}\rangle$ of electronic wave vector $\mathbf{k}$, representing a state where one electron is in subband $\lambda = 1$ is

$$|1, \mathbf{k}\rangle = c_{1\mathbf{k}}^{\dagger} c_{0\mathbf{k}} |F\rangle, \tag{1}$$

where $|F\rangle$ denotes the fundamental Fermi state (equilibrium state, where all the electrons are contained in subband $\lambda = 0$). For now, we restrain the problem to the $\lambda = 0, 1$ subbands, that form the intersubband optical transition. This transition will be denoted as α. Following the developments of Ref. [37], to describe the photoexcitation of an electron in the α transition, it is relevant to switch from

the fermionic basis formed by the $|1, \mathbf{k}\rangle$ states to a different basis of states $\{|B_i^{\alpha}\rangle\}_{i=[1:N]}$.

We have

$$|B_i^{\alpha}\rangle = \sum_{|\mathbf{k}| < \mathbf{k}_F} w_{i\mathbf{k}}^{\alpha} |1, \mathbf{k}\rangle. \tag{2}$$

Since the system is considered at $T = 0$ K, only $|\mathbf{k}| < \mathbf{k}_F$ states are occupied, $\mathbf{k}_F$ the module of the k wave vector corresponding to the Fermi level of the 0 subband. The $\{|B_i^{\alpha}\rangle\}_{i=[1:N]}$ basis covers only the single-excitation subspace (only one photoexcited electron per subband), which is sufficient in the case of a weak excitation regime. The coefficients $w_{i\mathbf{k}}^{\alpha}$ are defined as

$$w_{1\mathbf{k}}^{\alpha} = \frac{1}{\sqrt{N}} \quad \forall \, \mathbf{k}, \tag{3}$$

$$\sum_{\mathbf{k}} w_{i\mathbf{k}}^{\alpha} = 0 \quad \forall \, i \neq 1. \tag{4}$$

The $|B_1^{\alpha}\rangle$ state, of eigenenergy equal to the ISB transition energy $\omega_{\alpha} = \omega_1 - \omega_0$ (assuming parabolic dispersion), has the remarkable property of holding *the entire oscillator strength* of the α transition:

$$\langle F|\hat{d}|B_1^{\alpha}\rangle = z_{\alpha}\sqrt{N}, \tag{5}$$

where $\hat{d}$ denotes the dipole operator and z_{α} the dipole strength of one electronic transition. The $|B_1^{\alpha}\rangle$ state is called the *bright* state: it is formed by the *coherent* superposition of the one-particle fermionic states $|1, \mathbf{k}\rangle$ of the α transition and it holds the entire capacity of light-matter interaction. The $\{|B_i^{\alpha}\rangle\}_{i=[2:N]}$ are called the *dark* states since they cannot interact with the light:

$$\langle F|\hat{d}|B_i^{\alpha}\rangle = 0 \quad i \neq 1. \tag{6}$$

From these developments, one can define bright state destruction and creation operators b_{α} and $b_{\alpha}^{\dagger}$, which describe the collective excitation of the α transition:

$$b_{\alpha}^{\dagger} = \frac{1}{\sqrt{N}} \sum_{\mathbf{k}} c_{1\mathbf{k}}^{\dagger} c_{0\mathbf{k}}. \tag{7}$$

In a weak excitation regime and for a large number of electrons N, b_{α} can be approximated as a bosonic operator. b_{α} and $b_{\alpha}^{\dagger}$, respectively, demote and promote excitations inside the bright state $|B_1^{\alpha}\rangle$.

The final step in this development is to include the plasmonic effect ω_P of the electronic polarizations. The diagonalization of the plasmonic Hamiltonian leads to the emergence of new operators of eigenenergy $\tilde{\omega}_{\alpha} = \sqrt{\omega_{\alpha}^2 + \omega_P^2}$ and a plasmonic bright state that is still orthogonal to the

dark states [37]. Mathematically, this new state is essentially the same as the previous bright state, except that it is no longer degenerated with the dark states: for simplicity, we will keep the notation $|B_1^\alpha\rangle$ and b_α for, respectively, the bright state and the corresponding creation operator. Note: at this stage we did not introduce strong light-matter coupling yet. This derivation is therefore valid in any coupling regime.

B. Bosonization of the extractor: the tunnel-coupling Hamiltonian

We now turn to the insertion of the extraction subband in the formalism. As outlined in Refs. [19,38], the mixing of bosonic (the plasmonic ISB excitations) and fermionic (the electrons in the extraction subband) degrees of freedom is necessary to correctly model the transport mechanisms that take place in an optically excited ISB system. The focus of our paper is on ISB systems strongly coupled to a photonic mode, but we stress that the above consideration is valid also in the weak-coupling regime. When a photon is absorbed by an ISB transition, it generates a bosonic excitation: an ISB plasmon. But the measured current, in a detector, is of course of fermionic nature.

In the case where the extraction subband is explicitly included in the system dynamics (and not only in the form of an external bath), it becomes an extremely tedious task to keep track of all these degrees of freedom. Effectively, one correct way to describe the interaction between these excitations of a different nature is to use a full fermionic Hamiltonian of extremely large dimension. It is a significant mathematical challenge that demands considerable effort, and the nature of transport cannot be straightforwardly interpreted due to this complexity.

In this work, we overcome this strong limitation with a key modification: we propose to depict the subband $\lambda = 2$ with a bosonic operator in the context of an extraction process. This approach has several advantages, and—as we will discuss later on—it might also permit the scenario involving an injection process to be addressed. To explicitly incorporate subband $\lambda = 2$ into our formalism, we introduce the one-particle fermionic states $|2, \mathbf{k}\rangle$ of the β transition:

$$|2, \mathbf{k}\rangle = c_{2\mathbf{k}}^\dagger c_{0\mathbf{k}}|F\rangle. \tag{8}$$

Analogous to the α transition, we will not use this fermionic state basis and instead employ different orthonormal basis $\{|B_i^\beta\rangle\}_{i=[1:N]}$ defined as

$$|B_i^\beta\rangle = \sum_{|\mathbf{k}|<\mathbf{k}_F} w_{i\mathbf{k}}^\beta |2, \mathbf{k}\rangle, \tag{9}$$

where the coefficients $w_{i\mathbf{k}}^\beta$ are chosen such that

$$w_{1\mathbf{k}}^\beta = \frac{1}{\sqrt{N}} \quad \forall k, \tag{10}$$

$$\sum_k w_{i\mathbf{k}}^\beta = 0 \quad \forall i \neq 1. \tag{11}$$

The construction of this basis follows a similar approach as that of the $\{|B_i^\alpha\rangle\}_{i=[1:N]}$ basis. Specifically, the first state $|B_1^\beta\rangle$ is the bright state of the β transition, while the remaining states $\{|B_i^\beta\rangle\}_{i=[2:N]}$ are the dark states of this same transition. However, this time, the oscillator strength of a diagonal transition being very small, we have $z_\beta \ll z_\alpha$ and thus the bright and dark states of the extractor are degenerated. Note that the one excitation subspace describing subband 1 and 2, of dimension $2N$, is spanned by the concatenation of the $\{|B_i^\alpha\rangle\}_{i=[1:N]}$ and $\{|B_i^\beta\rangle\}_{i=[1:N]}$ basis.

The introduction of this alternative basis is valuable to evaluate the tunnel coupling between subbands 1 and 2 within the regime of strong light-matter coupling. The tunnel coupling operator $\hat{T}$ [39,40] can be defined as

$$\hat{T} = \Omega_T \sum_{\mathbf{k}} (c_{2\mathbf{k}}^\dagger c_{1\mathbf{k}} + c_{2\mathbf{k}}^\dagger c_{1\mathbf{k}}), \tag{12}$$

where Ω_T is the tunnel coupling strength. Using Eqs. (3), (4), (10), and (11), we compute the tunnel interaction between subbands 1 and 2:

$$\langle B_1^\alpha|\hat{T}|B_1^\beta\rangle = \Omega_T, \tag{13}$$

$$\langle B_1^\alpha|\hat{T}|B_j^\beta\rangle = 0 \quad j \neq 1, \tag{14}$$

$$\langle B_i^\alpha|\hat{T}|B_1^\beta\rangle = 0 \quad i \neq 1, \tag{15}$$

$$\langle B_i^\alpha|\hat{T}|B_j^\beta\rangle = \Omega_T \sum_{\mathbf{k}} w_{i\mathbf{k}}^{\alpha*} w_{j\mathbf{k}}^\beta \quad i \neq 1, j \neq 1. \tag{16}$$

The above relations, that are *de facto* selection rules, are one of the key results of this work: through tunnel interaction, it is not possible to transition from a dark state to a bright state [Eq. (14)] or vice versa [Eq. (15)]. Obviously, dark states can interact with each other through tunnel coupling [Eq. (16)], and the same applies to bright states as well [Eq. (13)].

These results have crucial implications on the nature of electronic transport in a QCD. For a detection process, where light promotes excitations into the $|B_1^\alpha\rangle$ bright state, the previous results suggest that an optical excitation can generate an electronic current in only two ways:

(1) Direct tunneling into the extractor bright state $|B_1^\beta\rangle$, preserving the coherent nature of the excitation, and subsequent decay—with loss of coherence—into an extractor dark state $|B_{i \neq 1}^\beta\rangle$ or

(2) First decay—with loss of coherence—into an ISB dark state $|B_{i \neq 1}^{\alpha}\rangle$ in the active region, and subsequent tunneling into an extractor dark state $|B_{i \neq 1}^{\beta}\rangle$.

Other channels involving bright-to-dark tunneling should not be considered, as they are prohibited by selection rules (14) and (15). Once in the extractor dark states, the electronic excitation will simply decay in the remaining cascade, generating photocurrent. We stress that the construction of the alternative β basis merely extended the procedure applied to the α transition (detailed in Ref. [37]) to the β transition, without additional hypothesis. By implementing this basis transformation, the comprehension of the transport process is streamlined, leading to the natural emergence of the selection rules presented in Eqs. (13) to (16). In the following section, we will assess the need to actually incorporate the dark states from both the α and β transitions to replicate the experimental photocurrent measurements from a QCD operating in the strong light-matter coupling regime. The implications of this section for an electronic injection process into polaritonic states will be discussed in Sec. IV.

C. Introducing dissipation and decoherence in the model

In the following, we develop an effective density-matrix model of the photocurrent extraction. We apply a drastic choice in the description of the system: we limit the extraction model to the transport induced by the bright states $|B_1^{\alpha}\rangle$ and $|B_1^{\beta}\rangle$. The dark states from both the α and β transitions are omitted. Both subbands 1 and 2 will thus be described using only bosonic operators. This is equivalent to choose scenario (1) among the two described at the end of the previous section: direct tunneling into the extractor bright state $|B_1^{\beta}\rangle$ (preserving the coherent nature of the excitation), and subsequent decay—with loss of coherence—into an extractor dark state $|B_{i \neq 1}^{\eta}\rangle$. This choice was already implicit in the approach that we have employed in our previous work based on a *classical* description of the electronic transport, using coupled mode theory [27].

We now go beyond this classical model using a quantum master equation. The key addition is the introduction of *decoherence* in the system, that is distinct from dissipation. In terms of spectral effects, decoherence impacts the broadening of the photocurrent peaks, while dissipation primarily affects their amplitude. In the experimental study we will report in Sec. III, bias will be varied, and—as a result—the amplitude of the peaks will be affected more than their broadening. It will be essential to differentiate between the effects of decoherence and dissipation, a distinction that was previously impossible to achieve with the classical model.

We define the operator b_{β} using our new basis from Eqs. (9) and (10):

$$b_{\beta}^{\dagger} = \frac{1}{\sqrt{N}} \sum_{\mathbf{k}} c_{2\mathbf{k}}^{\dagger} c_{0\mathbf{k}}, \tag{17}$$

$$b_{\beta}^{\dagger}|F\rangle = |B_1^{\beta}\rangle. \tag{18}$$

Using the fermionic commutation rules and a weak excitation regime, we have

$$[b_{\beta}, b_{\beta}^{\dagger}] = \frac{\hat{N}_0 - \hat{N}_2}{N} \approx \hat{\mathcal{I}}_d, \tag{19}$$

where $\hat{N}_i$ is the population operator of subband i and $\hat{\mathcal{I}}_d$ the identity operator. b_{β} can thus be approximated as a bosonic operator: b_{β} and $b_{\beta}^{\dagger}$ describe the destruction and creation of electronic excitations inside the extraction mode, of eigenfrequency $\omega_{\beta} = \omega_2 - \omega_0$. The related Hamiltonian is

$$\hat{\mathcal{H}}_{\beta} = \omega_{\beta} b_{\beta}^{\dagger} b_{\beta}. \tag{20}$$

We restrict the tunnel interaction to the interaction between the plasmonic bright mode and this new extraction mode. This drastically simplifies the tunnel interaction Hamiltonian described in Eq. (13). The restricted Hamiltonian $\hat{T}_{\text{bright}}$ is

$$\hat{T}_{\text{bright}} = \Omega_T (b_{\alpha}^{\dagger} b_{\beta} + b_{\alpha} b_{\beta}^{\dagger}). \tag{21}$$

The TM_{01} electromagnetic mode confined in the patch antennas will be modeled as a standard optical resonator of frequency ω_c, using a_c and $a_c^{\dagger}$ bosonic destruction and creation operators. Using the rotating-wave approximation to describe the light-matter interaction, the time-dependent Hamiltonian $\mathcal{H}(t)$ of the whole system reads

$$\begin{aligned}
\hat{\mathcal{H}}(t) = {} & \omega_c a_c^{\dagger} a_c + \tilde{\omega}_{\alpha} b_{\alpha}^{\dagger} b_{\alpha} + \omega_{\beta} b_{\beta}^{\dagger} b_{\beta} \\
& + \Omega \left(a_c^{\dagger} b_{\alpha} + a_c b_{\alpha}^{\dagger} \right) + \Omega_T \left(b_{\alpha}^{\dagger} b_{\beta} + b_{\alpha} b_{\beta}^{\dagger} \right) \\
& + \kappa_c s_+ \left(a_c e^{i\omega t} + a_c e^{-i\omega t} \right),
\end{aligned} \tag{22}$$

where s_+ is the amplitude of the incoming light excitation, ω its frequency, and κ_c is the coupling constant between this external field and the confined optical mode inside the cavity.

We map this system on an equivalent open quantum system described by the reduced density matrix ρ. Under standard Born-Markov approximations, the time evolution of the density matrix ρ obey the following quantum master

equation [41] ($\hbar = 1$ for clarity):

$$\frac{d\rho(t)}{dt} = -i[\mathcal{H}(t), \rho] + \gamma_\alpha \mathcal{L}[b_\alpha, \rho]$$
$$+ \gamma_\beta \mathcal{L}[b_\beta, \rho] + (\gamma_c + \Gamma_c)\mathcal{L}[a_c, \rho]$$
$$+ \gamma_\alpha^{\text{intra}} \mathcal{L}[b_\alpha^\dagger b_\alpha, \rho] + \gamma_\beta^{\text{intra}} \mathcal{L}[b_\beta^\dagger b_\beta, \rho], \quad (23)$$

where the $\mathcal{L}$ are Lindblad superoperators modeling the dissipative and decoherent interactions of the environment with the system. For any operator $\hat{A}$, a superoperator $\mathcal{L}$ reads

$$\mathcal{L}[\hat{A}, \rho] = 2\hat{A}\rho\hat{A}^\dagger - (\hat{A}^\dagger \hat{A}\rho + \rho\hat{A}^\dagger \hat{A}). \quad (24)$$

The plasmonic ISB excitations are mainly dissipated through their interaction with interface roughness, at a nonradiative rate γ_α. Similarly, the extractor dissipates electrons into the next period at a nonradiative rate γ_β, and is responsible for the generation of electrical current inside the structure. γ_β represents an effective dissipation rate that takes into consideration the remaining electronic cascade. The cavity also dissipates photons (mainly through undesired free-carrier absorption) at a rate γ_c, but also through a spontaneous emission channel, at a radiative rate Γ_c. Note that the radiative coupling κ_c is related to the radiative damping through $\kappa_c = \sqrt{2\Gamma_c}$ [42].

The main difference with our previous work [27] lies in the ability to explicitly introduce the *intrasubband* scattering through the pure decoherence terms $\gamma_\alpha^{\text{intra}} \mathcal{L}[b_\alpha^\dagger b_\alpha, \rho]$ (respectively, $\gamma_\beta^{\text{intra}} \mathcal{L}[b_\beta^\dagger b_\beta, \rho]$) [43]. These terms model pure decoherence damping without excitation dissipation (the intrasubband scattering thermalize excitations inside a subband without dissipating them into an other subband). By using the density-matrix formalism, it thus becomes possible to differentiate between the effects of intersubband (dissipation) and intrasubband (pure decoherence) processes on the evolution of the system (and ultimately on the shape of the calculated photoresponse spectra). More details on the necessity to distinguish intra- and intersubband scatterings can be found in Sec. 1 within the Supplemental Material [44].

D. Deriving observable quantities for comparison with experiments

Equation (23) can be solved numerically in steady state. The solution is a stationary reduced density matrix ρ_S, and any observable $\hat{O}$ can then be computed using

$$\langle \hat{O} \rangle = \text{Tr}(\hat{O}\rho_s), \quad (25)$$

where Tr represents the trace function. We can then compute the different interesting quantities of the system. The system total absorption is the sum of the power dissipated into the different decay channels, normalized by the incoming power $|s_+|^2$:

$$\mathcal{A}_{\text{tot}} = \mathcal{A}_c + \mathcal{A}_\alpha + \mathcal{A}_\beta \quad (26)$$

$$= 2\gamma_c \frac{\langle a_c^\dagger a_c \rangle}{|s^+|^2} + 2\gamma_\alpha \frac{\langle b_\alpha^\dagger b_\alpha \rangle}{|s^+|^2} + 2\gamma_\beta \frac{\langle b_\beta^\dagger b_\beta \rangle}{|s^+|^2}, \quad (27)$$

where $\mathcal{A}_c$, $\mathcal{A}_\alpha$, and $\mathcal{A}_\beta$ represent, respectively, the cavity, ISB, and extraction absorptions.

The net photocurrent $\mathcal{J}_\beta$ is defined as the current under illumination. $\mathcal{J}_\beta$ is proportional to the power dissipated from a period to the next adjacent period. This is exactly the power dissipated by the extraction mode β:

$$\mathcal{J}_\beta = 2\gamma_\beta \langle b_\beta^\dagger b_\beta \rangle. \quad (28)$$

Note: this is a phenomenological interpretation of the photocurrent. It is in fact expected that an excitation inside the bright extractor state $|B_1^\beta\rangle$ should first decay in the dark states $|B_{i\neq1}^\beta\rangle$ before being extracted in the electronic cascade and contribute to the photocurrent. We choose to neglect these dark extractor states such that the power is directly dissipated from the bright extractor state. This also applies on the ISB dissipation, where the $|B_{i\neq1}^\alpha\rangle$ dark states are neglected when considering the nonradiative dissipation γ_α.

III. EXPERIMENTAL VALIDATION IN PHOTODETECTION: THE POLARITON-TO-CURRENT PROCESS

A. Experimental details

The samples investigated in this study are the same as those already studied in Ref. [27]. They are processed into 8×8 (approximately equal to $50 \times 50 \, \mu\text{m}^2$) patch antenna arrays, with the patches connected through 250-nm thin metallic wires (see Fig. S3 within the Supplemental Material [44]). Details of the processing can be found in Ref. [45]. The samples are cooled down to $T = 78$ K in a cryostat, and they are illuminated by light from a globar source at normal incidence. The photocurrent spectra are acquired in rapid scan mode, after amplification using a low-noise transimpedance amplifier.

A summary of the samples' peak absorption and peak detection as a function of the detuning between cavity and ISB resonance is reported in Fig. 2. A few key features are apparent. (i) The anticrossing between cavity and ISB excitation, evidence of strong light-matter coupling, is apparent in absorption and also in photodetection. The photodetector does operate in the strong-coupling regime, as reported already in our previous works, Refs. [26,27].

(ii) The relative peak amplitudes do not anticross at the same cavity-ISB detuning in absorption and photodetection. It reveals that, as already pointed out in our previous works, Refs. [26,27,46], to faithfully model the relation between photocurrent and absorption in the strong-coupling regime, it is necessary to go beyond semiclassical models. It is the scope of this paper. We extended the data presented in Ref. [27], and now present measurements with voltage bias applied to the samples. The applied electric field ranges from $F = -25$ kV cm^{-1} to $F = 8$ kV cm^{-1}. We have fabricated several array designs (p, s), with p the interpatch period of the array, and s the lateral dimensions of the patches. However, to allow for a quantitative comparison, we present measurements under an applied electric field for two samples only, with same $p = 7$ μm, and $s = 1.5$ μm and $s = 1.55$ μm, respectively, as reported in Fig. 3 (continuous lines). Additional measurements can be found in Fig. S5 within the Supplemental Material [44]. While the relative amplitude of the spectra when varying the bias contains meaningful information of the electronic transport, one should exercise caution when comparing the amplitudes of different pairs (p, s) as the experimental protocol does not ensure a consistent illumination between each measurement of the device.

Two photocurrent peaks are clearly visible in Fig. 3, signature of the strong light-matter coupling regime. Note: the peaks under consideration cannot be confused with the two peaks arising from coupled subbands (tunnel coupling), since the peak positions would change with the applied bias in the latter case. Here, the energy splitting (for a given pair p, s) is constant regardless of the applied field. For all (p, s) couples studied, the global amplitude of the photocurrent spectra evolves with the applied electric field F. A maximum amplitude is observed around $F = -10$ kV cm^{-1}. The noise level increases strongly when the absolute amplitude of the field $|F|$ increases. The noise level is the direct consequence of the increase of the parasitic dark current with the electric field and—as is well known [47,48]—it affects the range of exploitable field F for device applications.

The relative amplitude of these peaks inverts with respect to the applied field F, with the equal amplitude condition of the two polaritonic photodetection peak found for a negative field $F \approx -5$ kV cm^{-1}. Below this threshold, the low-energy peak dominates. Inversely, for $F > -5$ kV cm^{-1}, it is the high-energy peak that dominates. This phenomenon can be attributed to the realignment of the subbands under the influence of the applied bias. When a highly negative voltage is applied, the subbands follow a clear staircase structure (see Fig. S4 within the Supplemental Material for the QCD band structure [44]), which facilitates the extraction process. Conversely, at positive voltages, the subband cascade becomes less organized, hindering the extraction process.

B. System parameters and constraints

Before applying the theoretical developments of Sec. II to the experimental data, let us detail the system parameters and the constraints applied to them.

The photonic degrees of freedom are the cavity parameters ω_c, γ_c, and Γ_c, that are independent of the applied electric field F. They only depend on the geometrical parameters (p, s) of the cavities [49–51]:

$$\omega_c(s) = \frac{\pi c_0}{n_{\text{eff}}s}, \tag{29}$$

$$\Gamma_c(p) = \frac{\alpha_c}{p^2}, \tag{30}$$

where c_0 is the light velocity, n_{eff} is the effective index of the cavity, that represents the effective medium composed of the semiconductor contacts and of the undoped periodic structure embedded between the gold layers forming that cavity, and α_c is the cavity dispersion loss factor. We choose to constrain n_{eff}, α_c, and γ_c to the values obtained from our prior investigation of the same samples [27], where the photocurrent of several samples with different (s,p) couples have been studied for $F = 0$ kV cm^{-1}:

$$n_{\text{eff}} = 3.22, \tag{31}$$

$$\alpha_c = 29.1 \text{ meV } \mu\text{m}^2, \tag{32}$$

$$\gamma_c = 3.4 \text{ meV}. \tag{33}$$

The cavity parameters are thus excluded from the fitting process.

Several electronic degree of freedom can also be fixed or constrained independently of our density-matrix model. The parameters of the ISB transition in the active QW (α) are assumed independent of the applied electric field F: the transition is vertical in a single quantum well and therefore is very marginally affected by the applied bias. The ISB frequency ω_α and the plasma frequency ω_P could be computed from our sequential transport software [34]. However, it is common to observe disparities between expected and measured doping levels (up to 15%). Experimental discrepancies also affect the ISB frequency (up to 5%), usually caused by the quality of the quantum well interfaces during the epitaxial process. To account for these disparities, and since both ω_α and ω_P are crucial parameters to reproduce the strong coupling measurements, we chose to let these parameters free during the fitting process:

$$\tilde{\omega}_\alpha = \sqrt{\omega_\alpha^2 + \omega_P^2}. \tag{34}$$

Note: the light-matter coupling constant Ω is parametrized using ω_P:

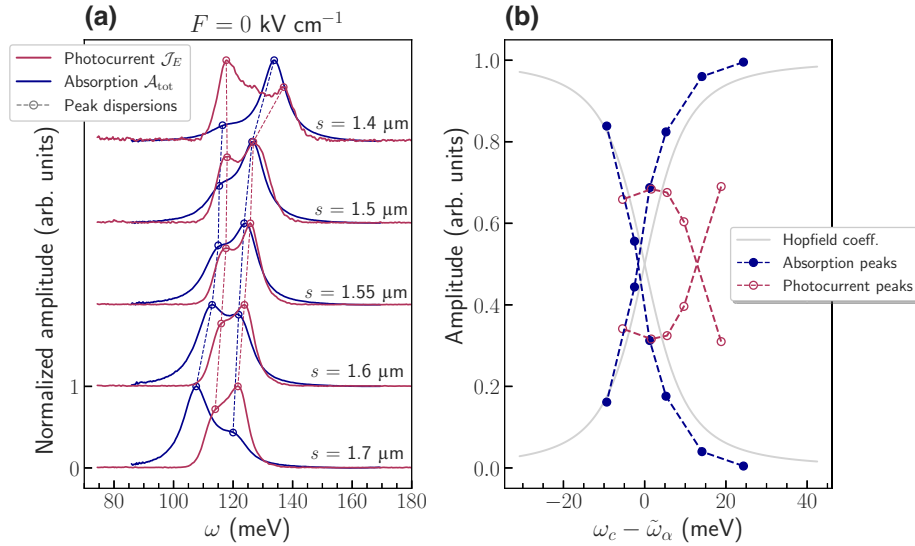$$\Omega = \frac{\omega_P}{2}\sqrt{f_w}, \tag{35}$$

FIG. 2. (a) Reflectivity measurements (blue) represented in the form of normalized absorption $\mathcal{A}_{\text{tot}} = 1 - \mathcal{R}$ and normalized photocurrent $\mathcal{J}_E$ measurements, for different patch sizes s. Offsets are added for visibility. The dashed lines represent the dispersion of the peak amplitudes, for both the absorption and the photocurrent. (b) Relative peak amplitudes for both the absorption and the photocurrent, with respect to the cavity-ISB detuning. The Hopfield coefficients (gray lines), extracted from the upcoming computations presented in Sec. III C, are superimposed on the figure.

with $f_w (\approx 0.17)$, the computed overlap factor between the cavity field and the doped active quantum wells.

Two additional α parameters can be computed using our sequential transport software: the nonradiative dissipation rate γ_α of the α plasmon from the excited subband to the fundamental subband, and the tunnel coupling Ω_T. We compute $\gamma_\alpha = 0.66$ meV and $\Omega_T = 4.2$ meV, respectively. The other key parameter of our transport model in the strong coupling regime, the intrasubband rate $\gamma_\alpha^{\text{intra}}$, will instead be fitted.

The parameters related to the extractor β are instead dependent on the electric field F: the extractor energy shifts with respect to the upper excited state of the ISB transition when a bias is applied to the structure. The misalignment is approximated as linear:

$$\omega_\beta(F) = \alpha_F F + \omega_\beta^0, \tag{36}$$

where α_F is the linear coefficient and ω_β^0 is the extractor energy for $F = 0$. This dispersion can be computed using our sequential transport software and is injected into the model:

$$\alpha_F = 1.12 \text{ meV}/(\text{kV cm}^{-1}), \tag{37}$$

$$\omega_\beta^0 = 124 \text{ meV}. \tag{38}$$

Similarly to $\gamma_\alpha^{\text{intra}}$, $\gamma_\beta^{\text{intra}}$ will be a fitting parameter common to the whole data set.

Finally, we expect the misalignment of the cascade with the electric field to modify the value of the effective extraction rate $\gamma_\beta(F)$. γ_β is one of the most significant parameters of the fitting process, as it controls the relative amplitude of the spectra. Although we suspect that it might closely match with the actual extraction rate calculated from our sequential transport model, we decided to keep it as a free parameter: for each measured electric field value F_i, we fit one extraction rate $\gamma_\beta(F_i)$. Note: $\gamma_\beta(F_i)$ is independent of the geometrical parameters p and s. In summary, ω_α, ω_P and $\gamma_\alpha^{\text{intra}}$ and $\gamma_\beta^{\text{intra}}$ are fitting parameters common to the whole data set, and their initial values for the fit will be based on the ones derived by our software.

C. Discussion on the validity of the fit

In this section, we perform a global fit on the whole experimental photocurrent dataset (Fig. 3), using the parameter constraints exposed in the previous section. We solve Eq. (23) in the stationary regime (using the QuTiP python library [52]) to evaluate the theoretical photocurrent J_β, as per Eq. (28). The parameters resulting from the fit are presented in Table I.

The returned values are consistent with the previous fits performed with the coupled mode theory in Ref. [27]. In particular, the extraction rate γ_β as a function of the applied electric field is plotted in Fig. 4 and compared with the values computed through our sequential transport model. The right order of magnitude is obtained ($\gamma_\beta < 1$ meV) and the evolution trends are relatively well reproduced (γ_β decreasing for $F > 0$, slope break around
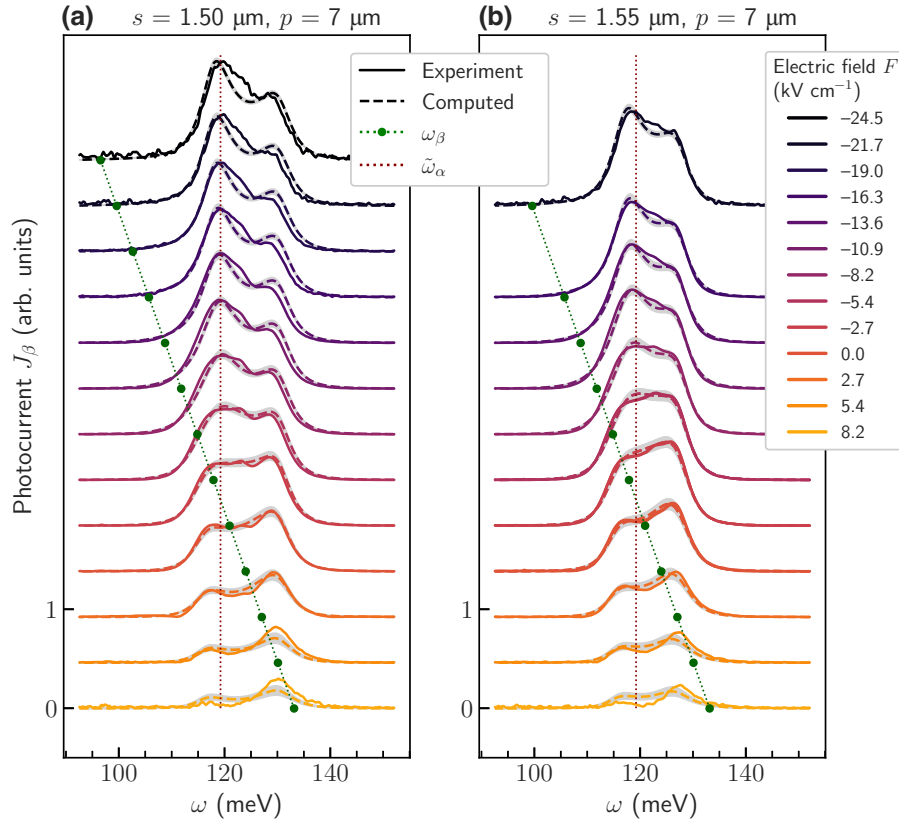
FIG. 3. Normalized photocurrent measurements (continuous lines) and quantum master equation global fit (dashed lines), for two cavity geometries (a) $s = 1.50\,\mu m$, $p = 7\,\mu m$ and (b) $s = 1.55\,\mu m$, $p = 7\,\mu m$. The same offsets are applied to both the experimental and computed spectra. These offset values are directly proportional to the bias applied to the structure and solely employed to distribute the curves vertically with even gaps in order to obtain a visually clear figure. Filled gray areas represent the errors of the fit parameters propagated onto the spectra. Note that in the case of the high-amplitude spectra, the errors exhibit minimal extension on the figure and are challenging to discern. The extractor frequency $\omega_\beta(F)$, dependant of the electric field F, and the plasma-shifted ISB transition $\tilde{\omega}_\alpha$ are both superimposed on the spectra. Additional results can be found in Fig. S5 within the Supplemental Material [44].

$F = -4$ kV cm^{-1}). These results on γ_β are also consistent with the evolution of the integrated amplitude of the spectra (Fig. 4, right-side scale): when the electric field is below $F = -4$ kV cm^{-1}, the electronic cascade is efficiently aligned, and the effective extraction rate γ_β is high. This leads to a significant photocurrent signal.

The spectrally resolved photocurrent calculated using the parameters returned by the global fit procedure is compared to the experimental data in Fig. 3. For each cavity configuration (p,s), we normalize both the experimental and computed spectra obtained with different bias using to

TABLE I. Parameters returned by the global fit using a quantum master equation model.

Fit parameters	Fit results
ω_α (meV)	116.9 ± 0.1 meV
γ_α^{intra} (meV)	2.4 ± 0.1 meV
γ_β^{intra} (meV)	9.3 ± 0.1 meV
ω_P (meV)	23.4 ± 0.1 meV

the maximum amplitude measured for this specific (p,s) configuration. This normalization enables a comparative analysis of the overall amplitude evolution with respect to the electric field F, for a specific set of (p,s) parameters. Using this method, we obtain a quantitative agreement on the set of triplets (p, s, F). Two key trends are reproduced as a function of the bias, i.e., as a function of the $\omega_\alpha - \omega_\beta$ alignment: (i) the amplitude ratio of the spectra between different bias conditions, and (ii) the relative amplitude inversion between the peaks of the two polaritonic branches. This study confirms that the extractor (the electronic cascade of the QCD) and its relative alignment with respect to the ISB transition controls the overall amplitude ratio of the spectra between different bias, as well as the relative amplitude of the peaks of the polaritonic branches. Applying an electric field to the structure enables the selective extraction of excitations from a polaritonic state towards the electronic cascade, while also providing control over the efficiency of this extraction. This selective extraction capacity is enabled by the sharp transfer function and the 2Ω spacing (the Rabi splitting)
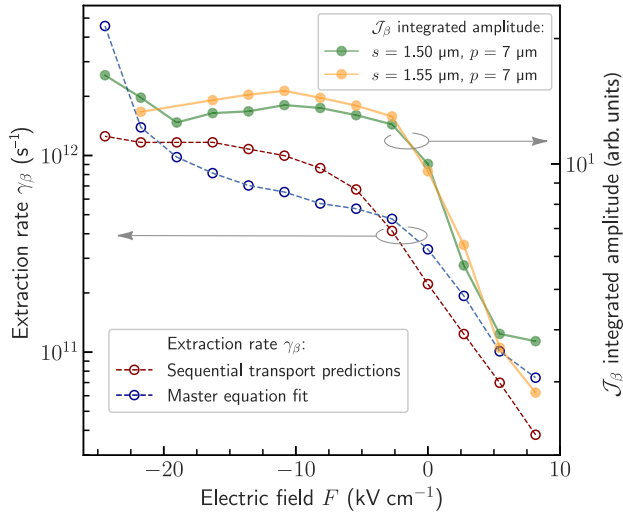
FIG. 4. Left-side scale: extraction rate γ_β as a function of the applied electric field F. Red cross: predicted values computed using a standard sequential transport model. Blue plus sign: values returned by the global fit using a quantum master equation model. Right-side scale: experimental photocurrent integrated amplitude, for two different (s, p) couples of cavity parameters.

between the polaritonic peaks: a finer transfer function and a stronger coupling would allow for better selectivity of $\omega_\pm$ polaritons. More details on a QCD transfer function in the strong-coupling regime can be found in Figs. S1 and S2 within the Supplemental Material [44].

The good agreement between the experimental data and the theoretical model provides strong evidence that the dark states for both transitions α and β do not need to be included in the model to depict an extraction process. The bright tunnel interaction $\hat{T}_{\text{bright}}$ and the phenomenological dissipation rate γ_β from the extractor bright state are sufficient to reproduce the experimental measurements. As previously postulated in Ref. [27], this result confirms that the polaritonic nature of the excitation is carried on during the extraction process through the coherent tunnel coupling. The extraction is a coherent process, mainly involving the bright states from both α and β transitions. This model permits however a step forward in the comprehension of the polariton-to-electron process. Chronologically, the early attempts were limited to the observation of a polariton splitting in photodetection [8,53]. A phenomenological transfer function was then introduced in the study of QWIPs operating in strong coupling [26]. Recently, the coupled-mode theory (CMT) permitted a more rigorous modeling of the transfer function, and an initial indication of direct tunneling into the extractor bright state, with no role for the polaritonic dark states [27]. The model presented in this paper gets rid of the transfer function—a phenomenological concept—and replaces it with a rigorous tunnel coupling Hamiltonian between the α and β transitions, with a complete description of bright and

dark states. The latter do not play a major role for the *polariton extraction* process, but they have a crucial role for *polariton injection*. Our model integrates them, and might constitute a valid vantage point to study electrically injected polariton emitters. More information on the transfer function and the difference between the CMT and the effective density-matrix approach can be found in Fig. S2 within the Supplemental Material [44].

IV. IMPLICATIONS OF THE MODEL FOR ELECTRICALLY PUMPED POLARITON EMITTERS: THE ELECTRON-TO-POLARITON PROCESS

The validity of the density-matrix approach to describe electrical *extraction* from optically excited polaritons, motivates us to study the implications of these findings on the electrical *injection* and subsequent photon emission, represented by the red arrows in Fig. 1. As discussed in Ref. [38], the main difficulty describing an intersubband emitter operating in the strong light-matter coupling regime lies in the simultaneous description of both optical (bosonic) and electronic (fermionic) excitations. The injection process fills subband 2 with fermionic excitations in the form of electrons, while the plasmonic excitations that occupy the α bright state are bosonic. Working with the full Fermionic Hamiltonian is an arduous task [38], that could hinder the development of an intuitive understanding of the transport, although very recently a Fermionic approach was successfully used to model QCDs operating in the strong-coupling regime [33].

The previous Sec. II B suggests that the bosonization procedure of the extractor, that we employed to describe the extraction process, is an effective and readily interpretable approach for examining the injection process. In particular the selection rules for the tunnel Hamiltonian, Eqs. (13)–(16) might prove a powerful tool. Due to the impossibility of conducting an experimental study resembling the one carried out for QCDs for a detection process, the following discussion will be supported by the quantitative arguments previously presented in Sec. II C. Note: the β extractor states are now referred to as *injector* states.

An injection process is inherently incoherent because it introduces electrical excitations into an intersubband system through an incoherent external bath of electrons.

The relevant *coherence* here is the one of the ISB plasmon [28–30], that is a collective—and coherent—matter excitation originating from the electronic plasma inside a semiconductor quantum well (QW). In this respect, an intuitive picture suggests that for an ISB polariton system, the electrical injection process is *not* the reverse of the electrical extraction. In the latter, coherence (induced by light) is destroyed to generate an electrical current, while in the former it appears that coherence must be created. More formally, in the framework of a bosonized injector, we

expect most of the electronic population to be located in the dark states $|B_i^\beta\rangle$ ($i \neq 1$) upon electrical injection. Furthermore, to emit light, excitations must be transferred to the plasmonic bright state $|B_1^\alpha\rangle$, which holds the entire oscillator strength of the system. However, the selection rules (14) and (15) are clear: it is impossible for a dark state from the injector to interact with the plasmonic bright state through a tunnel interaction. In other words, the primary injection pathway, which would involve direct transfer from the injector states to the bright plasmonic state, cannot be taken. The bosonized injector formalism confirms that *polaritonic emitters do not operate as reversed polaritonic detectors*.

In QCDs, the coherence is established through the photonic mode and maintained up to the extractor using both light-matter coupling Ω and tunnel coupling Ω_T. Coherence can also be lost through the irreversible intrasubband scatterings $\gamma_\alpha^{\text{intra}}$ in the plasmonic mode, although we have demonstrated that it is *not* the main extraction scheme. However, the extraction process can still take place, since the usual dark-to-dark tunnel interactions are possible [Eq. (16)]. In contrast, in a LED the injection mechanism is incoherent, and coherence cannot emerge spontaneously during the transport. Additionally, we showed that incoherent (dark) states cannot interact with a coherent (bright) *via* the tunneling Hamiltonian [Eq. (15)] and [Eq. (14)]. As a result, it seems unfeasible to efficiently transfer excitations to the optically active bright state α, and thus to the polaritonic states, in the absence of an additional mechanism to generate coherence.

In the case where the electrical injection would be uniform among the N states of $|B_i^\beta\rangle$, light could be emitted since the system would start with excitations in $|B_1^\beta\rangle$, but the expected efficiency would be at most $1/N$, without considering intrasubband decoherence.

There is however a point that needs to be discussed further. Several reports of electroluminescence from electrically injected polariton LEDs exist in the literature. Some of them clearly determine that thermally assisted emission processes have a major role [23,54], but in many other ones simple thermal models cannot explain the data [20–22,24]. We can only conjecture possible ways forward to elucidate electrical injection of polaritonic LEDs. On one hand, one might wonder if the application of the generalized, local Kirchoff [55] law to ISB polariton LEDs can shine light on the electrical injection process, and possibly explain all the existing experimental data in the literature. On the other, the problem of electrical excitation of coherent electronic motion—which is essentially the mechanism at play in electrically pumped polariton emitters—is well known from the field of surface plasmon polaritons (SPPs) [56–62]. The extremely low efficiency of the electron-to-plasmon and electron-to-photon processes is well known, although recent theoretical works, supported by one experimental finding, have

demonstrated that the efficiency could be drastically increased by tailoring the electronic landscape to favor inelastic over elastic tunneling, as long as the electronic coherence is preserved in the process [63,64].

Of note is the theoretical strategy employed in those works: while SPPs are bosons too, bosonization is in general not employed. Instead, the amplitude of the electron-to-SPP process is calculated using Fermi's golden rule in a Fermionic hamiltonian, as for instance in Ref. [63]. We speculate that the judicious combination of such approaches with the bosonization procedure presented in this work could lead to a quantitative evaluation of the electron-to-ISB polariton process efficiency.

[1] J. Kasprzak, M. Richard, S. Kundermann, A. Baas, P. Jeambrun, J. M. J. Keeling, F. M. Marchetti, M. H. Szymańska, R. André, J. L. Staehli, V. Savona, P. B. Littlewood, B. Deveaud, and L. S. Dang, Bose–Einstein condensation of exciton polaritons, Nature **443**, 409 (2006).

[2] D. Bajoni, E. Semenova, A. Lemaître, S. Bouchoule, E. Wertz, P. Senellart, and J. Bloch, Polariton light-emitting diode in a GaAs-based microcavity, Phys. Rev. B **77**, 113303 (2008).

[3] I. Carusotto and C. Ciuti, Quantum fluids of light, Rev. Mod. Phys. **85**, 299 (2013).

[4] E. Orgiu, J. George, J. A. Hutchison, E. Devaux, J. F. Dayen, B. Doudin, F. Stellacci, C. Genet, J. Schachenmayer, C. Genes, G. Pupillo, P. Samorì, and T. W. Ebbesen, Conductivity in organic semiconductors hybridized with the vacuum field, Nat. Mater. **14**, 1123 (2015).

[5] F. Appugliese, J. Enkner, G. L. Paravicini-Bagliani, M. Beck, C. Reichl, W. Wegscheider, G. Scalari, C. Ciuti, and J. Faist, Breakdown of topological protection by cavity vacuum fields in the integer quantum Hall effect, Science **375**, 1030 (2022).

[6] C. Ciuti, Cavity-mediated electron hopping in disordered quantum hall systems, Phys. Rev. B **104**, 155307 (2021).

[7] D. Dini, R. Köhler, A. Tredicucci, G. Biasiol, and L. Sorba, Microcavity polariton splitting of intersubband transitions, Phys. Rev. Lett. **90**, 116401 (2003).

[8] E. Dupont, H. C. Liu, A. J. SpringThorpe, W. Lai, and M. Extavour, Vacuum-field Rabi splitting in quantum-well infrared photodetectors, Phys. Rev. B **68**, 245320 (2003).

[9] S. De Liberato and C. Ciuti, Stimulated scattering and lasing of intersubband cavity polaritons, Phys. Rev. Lett. **102,** 136403 (2009).

[10] R. Colombelli and J.-M. Manceau, Perspectives for intersubband polariton lasers, Phys. Rev. X **5,** 011031 (2015).

[11] J.-M. Manceau, N.-L. Tran, G. Biasiol, T. Laurent, I. Sagnes, G. Beaudoin, S. De Liberato, I. Carusotto, and R. Colombelli, Resonant intersubband polariton-lo phonon scattering in an optically pumped polaritonic device, Appl. Phys. Lett. **112,** 191106 (2018).

[12] M. Knorr, J.-M. Manceau, J. Mornhinweg, J. Nespolo, G. Biasiol, N.-L. Tran, M. Malerba, P. Goulain, X. Lafosse, M. Jeannin, M. Stefinger, I. Carusotto, C. Lange, R. Colombelli, and R. Huber, Intersubband polariton-polariton scattering in a dispersive microcavity, Phys. Rev. Lett. **128,** 247401 (2022).

[13] J. Yu, S. Park, I. Hwang, D. Kim, F. Demmerle, G. Boehm, M.-C. Amann, M. A. Belkin, and J. Lee, Electrically tunable nonlinear polaritonic metasurface, Nat. Photonics **16,** 72 (2022).

[14] S. Pirotta, N.-L. Tran, A. Jollivet, G. Biasiol, P. Crozat, J.-M. Manceau, A. Bousseksou, and R. Colombelli, Fast amplitude modulation up to 1.5 GHz of mid-IR free-space beams at room-temperature, Nat. Commun. **12,** 799 (2021).

[15] S. A. Mann, N. Nookala, S. C. Johnson, M. Cotrufo, A. Mekawy, J. F. Klem, I. Brener, M. B. Raschke, A. Alù, and M. A. Belkin, Ultrafast optical switching and power limiting in intersubband polaritonic metasurfaces, Optica **8,** 606 (2021).

[16] M. Jeannin, J.-M. Manceau, and R. Colombelli, Unified description of saturation and bistability of intersubband transitions in the weak and strong light-matter coupling regimes, Phys. Rev. Lett. **127,** 187401 (2021).

[17] M. Jeannin, E. Cosentino, S. Pirotta, M. Malerba, G. Biasiol, J.-M. Manceau, and R. Colombelli, Low intensity saturation of an ISB transition by a mid-ir quantum cascade laser, Appl. Phys. Lett. **122,** 241107 (2023).

[18] R. Colombelli, C. Ciuti, Y. Chassagneux, and C. Sirtori, Quantum cascade intersubband polariton light emitters, Semicond. Sci. Technol. **20,** 985 (2005).

[19] S. De Liberato and C. Ciuti, Quantum model of microcavity intersubband electroluminescent devices, Phys. Rev. B **77,** 155321 (2008).

[20] L. Sapienza, A. Vasanelli, R. Colombelli, C. Ciuti, Y. Chassagneux, C. Manquest, U. Gennser, and C. Sirtori, Electrically injected cavity polaritons, Phys. Rev. Lett. **100,** 136806 (2008).

[21] P. Jouy, A. Vasanelli, Y. Todorov, L. Sapienza, R. Colombelli, U. Gennser, and C. Sirtori, Intersubband electroluminescent devices operating in the strong-coupling regime, Phys. Rev. B **82,** 045322 (2010).

[22] A. Delteil, A. Vasanelli, P. Jouy, D. Barate, J. C. Moreno, R. Teissier, A. N. Baranov, and C. Sirtori, Optical phonon scattering of cavity polaritons in an electroluminescent device, Phys. Rev. B **83,** 081404 (2011).

[23] D. Chastanet, J.-M. Manceau, T. Laurent, A. Bousseksou, G. Beaudoin, I. Sagnes, and R. Colombelli, Surface emitting thermally assisted polaritonic light-emitting device, Appl. Phys. Lett. **110,** 081108 (2017).

[24] M. Geiser, G. Scalari, F. Castellano, M. Beck, and J. Faist, Room temperature terahertz polariton emitter, Appl. Phys. Lett. **101,** 141118 (2012).

[25] B. Limbacher, M. A. Kainz, S. Schoenhuber, M. Wenclawiak, C. Derntl, A. M. Andrews, H. Detz, G. Strasser, A. Schwaighofer, B. Lendl, J. Darmo, and K. Unterrainer, Resonant tunneling diodes strongly coupled to the cavity field, Appl. Phys. Lett. **116,** 221101 (2020).

[26] P.-B. Vigneron, S. Pirotta, I. Carusotto, N.-L. Tran, G. Biasiol, J.-M. Manceau, A. Bousseksou, and R. Colombelli, Quantum well infrared photo-detectors operating in the strong light-matter coupling regime, Appl. Phys. Lett. **114,** 131104 (2019).

[27] M. Lagrée, M. Jeannin, G. Quinchard, O. Ouznali, A. Evirgen, V. Trinité, R. Colombelli, and A. Delga, Direct polariton-to-electron tunneling in quantum cascade detectors operating in the strong light-matter coupling regime, Phys. Rev. Appl. **17,** 044021 (2022).

[28] T. Ando, A. Fowler, and F. Stern, Electronic properties of two-dimensional systems, Rev. Mod. Phys. **54,** 437 (1982).

[29] M. Helm, *Intersubband Transitions in Quantum Wells: Physics and Device Applications I*, edited by H.C. Liu and F. Capasso (Academic Press, San Diego, 1999), 1st ed., Vol. 62, Chap.1, ISBN: 9780080864600.

[30] A. Delteil, A. Vasanelli, Y. Todorov, C. Feuillet Palma, M. Renaudat St-Jean, G. Beaudoin, I. Sagnes, and C. Sirtori, Charge-induced coherence between intersubband plasmons in a quantum structure, Phys. Rev. Lett. **109,** 246808 (2012).

[31] A. A. Khalifa, A. P. D. Love, D. N. Krizhanovskii, M. S. Skolnick, and J. S. Roberts, Electroluminescence emission from polariton states in GaAs-based semiconductor microcavities, Appl. Phys. Lett. **92,** 061107 (2008).

[32] S. I. Tsintzos, N. T. Pelekanos, G. Konstantinidis, Z. Hatzopoulos, and P. G. Savvidis, A GaAs polariton light-emitting diode operating near room temperature, Nature **453,** 372 (2008).

[33] F. Pisani, D. Gacemi, A. Vasanelli, L. Li, A. G. Davies, E. Linfield, C. Sirtori, and Y. Todorov, Electronic transport driven by collective light-matter coupled states in a quantum device, Nat. Commun. **14,** 3914 (2023).

[34] V. Trinité, E. Ouerghemmi, V. Guériaux, M. Carras, A. Nedelcu, E. Costard, and J. Nagle, Modelling of electronic transport in quantum well infrared photodetectors, Infrared Phys. Technol. **54,** 204 (2011).

[35] C. Koeniguer, G. Dubois, A. Gomez, and V. Berger, Electronic transport in quantum cascade structures at equilibrium, Phys. Rev. B **74,** 235325 (2006).

[36] A. Buffaz, A. Gomez, M. Carras, L. Doyennette, and V. Berger, Role of subband occupancy on electronic transport in quantum cascade detectors, Phys. Rev. B **81,** 075304 (2010).

[37] Y. Todorov and C. Sirtori, Intersubband polaritons in the electrical dipole gauge, Phys. Rev. B **85,** 045304 (2012).

[38] S. De Liberato and C. Ciuti, Quantum theory of electron tunneling into intersubband cavity polariton states, Phys. Rev. B **79,** 075317 (2009).

[39] R. Kazarinov and R. Suris, Electric and electromagnetic properties of semiconductors with a superlattice, Sov. Phys. Semicond. **6,** 120 (1972).

[40] H. Willenberg, G. Döhler, and J. Faist, Intersubband gain in a Bloch oscillator and quantum cascade laser, Phys. Rev. B **67**, 085315 (2003).

[41] H.-P. Breuer and F. Petruccione, *The Theory of Open Quantum Systems* (Oxford University Press, Oxford, 2002), 1st ed., ISBN: 9780199213900.

[42] W. Suh, Z. Wang, and S. Fan, Temporal coupled-mode theory and the presence of non-orthogonal modes in lossless multimode cavities, IEEE J. Quantum Electron. **40**, 1511 (2004).

[43] M. A. Schlosshauer, *Decoherence: and the Quantum-To-Classical Transition* (Springer Science & Business Media, Berlin, 2007), ISBN: 3540357734.

[44] See Supplemental Material at http://link.aps.org/supplemental/10.1103/PhysRevApplied.21.034002 for details on our quantum master equation model for QCD operating in the strong light-matter coupling regime (Sec. 1), information about our experimental system (Fig. S3) and QCD bandstructure (Fig. S4) and additional photocurrent measurements and computational results (Fig. S5).

[45] G. Quinchard, C. Mismer, M. Hakl, J. Pereira, Q. Lin, S. Lepillet, V. Trinité, A. Evirgen, E. Peytavit, J. Reverchon, *et al.*, High speed, antenna-enhanced 10.3 μm quantum cascade detector, Appl. Phys. Lett. **120**, 091108 (2022).

[46] M. Lagrée, *Transport électronique en régime de Couplage Fort Lumière-Matière Pour les Dispositifs Quantiques Moyen-Infrarouge* (Doctoral dissertation, Université Paris-Saclay, 2022).

[47] A. Delga, M. Carras, V. Trinité, V. Guériaux, L. Doyennette, A. Nedelcu, H. Schneider, and V. Berger, Master equation approach of classical noise in intersubband detectors, Phys. Rev. B **85**, 245414 (2012).

[48] M. Hakl, Q. Lin, S. Lepillet, M. Billet, J.-F. Lampin, S. Pirotta, R. Colombelli, W. Wan, J. C. Cao, H. Li, E. Peytavit, and S. Barbieri, Ultrafast quantum-well photodetectors operating at 10 μm with a flat frequency response up to 70 GHz at room temperature, ACS Photonics **8**, 464 (2021).

[49] Y. Todorov, L. Tosetto, J. Teissier, A. M. Andrews, P. Klang, R. Colombelli, I. Sagnes, G. Strasser, and C. Sirtori, Optical properties of metal-dielectric-metal microcavities in the THz frequency range, Opt. Express **18**, 13886 (2010).

[50] C. A. Balanis, *Antenna Theory: Analysis and Design* (John Wiley & Sons, New-York, 2016), 4th ed., ISBN: 978-1-118-64206-1.

[51] D. Palaferri, *Antenna Resonators for Quantum Infrared Detectors and Fast Heterodyne Receivers* (Doctoral dissertation, Sorbonne Paris Cité, 2018).

[52] J. R. Johansson, P. D. Nation, and F. Nori, Qutip: An open-source python framework for the dynamics of open quantum systems, Comput. Phys. Commun. **183**, 1760 (2012).

[53] L. Sapienza, A. Vasanelli, C. Ciuti, C. Manquest, C. Sirtori, R. Colombelli, and U. Gennser, Photovoltaic probe of cavity polaritons in a quantum cascade structure, Appl. Phys. Lett. **90**, 201101 (2007).

[54] B. Askenazi, A. Vasanelli, Y. Todorov, E. Sakat, J.-J. Greffet, G. Beaudoin, I. Sagnes, and C. Sirtori, Midinfrared ultrastrong light–matter coupling for THz thermal emission, ACS Photonics **4**, 2550 (2017).

[55] J.-J. Greffet, P. Bouchon, G. Brucoli, and F. m. c. Marquier, Light emission by nonequilibrium bodies: Local Kirchhoff law, Phys. Rev. X **8**, 021008 (2018).

[56] J. Lambe and S. L. McCarthy, Light emission from inelastic electron tunneling, Phys. Rev. Lett. **37**, 923 (1976).

[57] L. C. Davis, Theory of surface-plasmon excitation in metal-insulator-metal tunnel junctions, Phys. Rev. B **16**, 2482 (1977).

[58] P. Bharadwaj, A. Bouhelier, and L. Novotny, Electrical excitation of surface plasmons, Phys. Rev. Lett. **106**, 226802 (2011).

[59] M. Parzefall, P. Bharadwaj, A. Jain, T. Taniguchi, K. Watanabe, and L. Novotny, Antenna-coupled photon emission from hexagonal boron nitride tunnel junctions, Nat. Nanotechnol. **10**, 1058 (2015).

[60] J. Kern, R. Kullock, J. Prangsma, M. Emmerling, M. Kamp, and B. Hecht, Electrically driven optical antennas, Nat. Photonics **9**, 582 (2015).

[61] W. Du, T. Wang, H.-S. Chu, and C. A. Nijhuis, Highly efficient on-chip direct electronic–plasmonic transducers, Nat. Photonics **11**, 623 (2017).

[62] H. Qian, S.-W. Hsu, K. Gurunatha, C. T. Riley, J. Zhao, D. Lu, A. R. Tao, and Z. Liu, Efficient light generation from enhanced inelastic electron tunnelling, Nat. Photonics **12**, 485 (2018).

[63] A. V. Uskov, J. B. Khurgin, I. E. Protsenko, I. V. Smetanin, and A. Bouhelier, Excitation of plasmonic nanoantennas by nonresonant and resonant electron tunnelling, Nanoscale **8**, 14573 (2016).

[64] H. Qian, S. Li, S.-W. Hsu, C.-F. Chen, F. Tian, A. R. Tao, and Z. Liu, Highly-efficient electrically-driven localized surface plasmon source enabled by resonant inelastic electron tunneling, Nat. Commun. **12**, 3111 (2021).